# Seesaw of Tropical Cyclone Frequency between Eastern and Western Regions of the Western North Pacific

Kaiyue Shan,[a] Wenchao Chu,[b] Pao-Shin Chu,[c] and Xiping Yu[d]

[a] *State Key Laboratory of Hydroscience and Engineering, Department of Hydraulic Engineering, Tsinghua University, Beijing, China*
[b] *Lamont-Doherty Earth Observatory, Columbia University, Palisades, New York*
[c] *Department of Atmospheric Sciences, School of Ocean and Earth Science and Technology, University of Hawaiʻi at Mānoa, Honolulu, Hawaii*
[d] *Department of Ocean Science and Engineering, Southern University of Science and Technology, Shenzhen, China*

(Manuscript received 7 May 2024, in final form 7 January 2025, accepted 23 January 2025)

ABSTRACT: Because of the limited length of observed tropical cyclone (TC) data and low confidence in modeling TC genesis frequency, it has been difficult to understand why the genesis frequency of global TCs has remained nearly invariant while regional variations are highly pronounced. Investigating the covariability of TC genesis frequency between different regions may shed light on this question. Here, we identify that TC genesis frequency varies out of phase between the eastern and western regions of the western North Pacific (WNP). Such a seesaw relationship could be explained by the east–west dipole patterns of low-level vorticity and midtropospheric relative humidity in the WNP, associated with variations in atmospheric conditions. Composite analyses and numerical experiments show that a combination of cooling in the WNP and warming in the north Indian Ocean (NIO) exerts a significant influence on the seesaw pattern. Our study adds more evidence to believe on number conservation of worldwide TC genesis.

SIGNIFICANCE STATEMENT: Little had been known about why the genesis frequency of global tropical cyclones has remained nearly invariant in a changing climate. To find out whether there is any covariability of tropical cyclone genesis frequency between different regions may provide a chance to understand such a steady trend. The western North Pacific is the ocean basin where tropical cyclones are the most active in the world. In this study, it is observed that tropical cyclone genesis frequency between the eastern and western regions of the western North Pacific has a negative correlation. It is demonstrated that the zonal contrast of sea surface temperature in the western North Pacific to the north Indian Ocean plays a significant role in driving the seesaw relationship of tropical cyclone genesis frequency by moderating the large-scale atmospheric circulation.

KEYWORDS: Sea surface temperature; Tropical cyclones; Climate variability; Oceanic variability

## 1. Introduction

The genesis frequency of tropical cyclones (TCs) on Earth has remained nearly invariant at around 80, showing no clear trend of increasing or decreasing, despite the rising global mean temperature since the mid-twentieth century (Schreck et al. 2014; Murakami et al. 2020; Sobel et al. 2021). TC genesis frequency is perhaps the most poorly understood aspect regarding the climatological study of TCs. There is no accepted explanation for the changelessness of global TC genesis frequency (Walsh et al. 2015). In fact, neither modern instrumental observations nor paleo-proxy archives provide direct evidence for any long-term trend in global TC frequency yet. Numerical models, however, show inconsistency in modeling TC genesis frequency, both in their historical simulations and future projections. The theoretical base of this subject is still not well established (Sobel et al. 2021).

An effective approach to address this problem is to find out whether there is any covariability in TC genesis frequency among different ocean basins or among different regions within an ocean basin. In contrast to the steady trend of the global TC genesis frequency, the regional TC genesis frequency is characterized by considerable variability at the interannual and decadal time scales (Kim et al. 2010; Murakami et al. 2020; Shan and Yu 2020a,b; Chu and Murakami 2022; Wu et al. 2023). Many studies have shown that TC genesis frequency in the eastern North Pacific and North Atlantic Ocean varies out of phase (Maue 2009; Wang and Lee 2009; Wang et al. 2016; Chu and Murakami 2022). As the two regions are separated by Central America, this phenomenon is well known as a seesaw relationship of TC genesis frequency. There is also a correlation between the decreased TC genesis in the western North Pacific (WNP) and the increased TC genesis in the North Atlantic Ocean (Wang et al. 2022; Cao et al. 2023a; Huang et al. 2023). Kim et al. (2010) further explored this concept, identifying a dipole oscillation in TC genesis between the Philippine Sea and the northern South China Sea at both interannual and interdecadal time scales. Cao et al. (2023b) focused on a significant out-of-phase variation between spring (March–May) TC genesis over the eastern part of the WNP and the subsequent summer–fall (June–November) TC

Supplemental information related to this paper is available at the Journals Online website: https://doi.org/10.1175/JCLI-D-24-0255.s1.

*Corresponding author*: Xiping Yu, yuxp@sustech.edu.cn

DOI: 10.1175/JCLI-D-24-0255.1

genesis over the South China Sea. Moreover, an out-of-phase variation in TC genesis frequency is found between the Arabian Sea and the Bay of Bengal–South China Sea (Yuan et al. 2019; Cao et al. 2023c). Investigating the covariability of TC genesis frequency between different regions and the underlying mechanisms may shed some light on the phenomenon of number conservation of worldwide TC genesis frequency.

The WNP is the ocean basin where TCs are the most active in the world, accounting for about one-third of the total number. It may be divided into two regions, i.e., the eastern and the western regions, by the Philippine Islands. There are significant differences in the properties of TCs between the two regions of the WNP (Kim et al. 2010; Ling et al. 2015; Wu et al. 2019; Shan and Yu 2020a; Tu et al. 2022; Shan et al. 2023; Li and Mei 2024). Based on the aforementioned studies, the objective of the current study is to provide further evidence for an out-of-phase relationship between TC genesis frequencies over the eastern and western regions of the WNP. We do find a seesaw relationship of TC genesis frequency between these two regions of the WNP at the interannual time scale. We then explore the underlying mechanisms for such a seesaw relationship.

## 2. Data and methods

The TC dataset over the WNP is obtained from the International Best Track Archive for Climate Stewardship v04r00 (Knapp et al. 2010). Note that the records of TC genesis frequency are generally consistent in different datasets even back to the presatellite era, while the records of TC intensity have discrepancies (Kossin et al. 2007; Wang et al. 2022). TC genesis is defined as the initial record point of a TC that attains a maximum sustained wind speed of 35 kt (1 kt $\approx$ 0.51 m s$^{-1}$) or greater during its lifetime. The fifth major global reanalysis produced by the European Centre for Medium-Range Weather Forecasts (Hersbach et al. 2020) provides atmospheric variables on a monthly scale. The Extended Reconstructed Sea Surface Temperature, version 5, dataset is used to derive sea surface temperature on a monthly scale (Huang et al. 2017). The eastern and western regions of the WNP are roughly divided by the Philippine Islands. The eastern region of the WNP is defined as the domain of 130°–170°E and 0°–20°N, and the western region of the WNP is defined as the domain of 105°–130°E and 0°–25°N, including the South China Sea and the Philippine Sea. The longitude of 130°E also coincides with the position of the ascending branch of the Walker circulation, which plays a dominant role in modulating background atmospheric conditions in the WNP (Shan and Yu 2021; Chen et al. 2022).

To identify the difference between positive and negative phases in the two regions, five active TC years for the eastern region of the WNP (1987, 1993, 2003, 2011, and 2018) and five active TC years for the western region of the WNP (1984, 1994, 1999, 2013, and 2017) are selected as representative years, referred as the eastern active years and the western active years, respectively. The selection of representative active years was based on the criterion that TC genesis frequency during these years exceeded the long-term average. Specifically, for the western region of the WNP, the year is selected if the TC genesis frequency equals or exceeds five, while for the eastern region of the WNP, the threshold is set at nine. Additionally, years before 1979 were excluded from the analysis to avoid uncertainties associated with the less reliable satellite observations and environmental data from the 1970s. To ensure a balanced representation across different periods, a minimum interval of 3 years was maintained between selected years to prevent any bias that could arise from closely spaced years within the same time window. Note that our conclusions are consistent even when a different number of representative years is selected (Fig. S1 in the online supplemental material). To ensure the robustness of these results, we also calculated the difference between inactive TC years for the eastern region of the WNP and those for the western region. The representative inactive years were selected using the same criteria as outlined above, with the adjustment that TC genesis frequency during these years was below the long-term average. A similar conclusion can be drawn from the analysis of these inactive years (Fig. S2), further supporting the overall findings.

To investigate the effect of ENSO phases on the robustness of the results, a parallel composite analysis was conducted with ENSO years excluded. The ENSO years are defined as those with sea surface temperature (SST) anomalies in the Niño-3.4 region exceeding ±0.5°C during the peak season (July–September). After excluding these years, five non-ENSO active TC years were identified for the eastern region of the WNP (1989, 1993, 1996, 2003, and 2018) and five for the western region of the WNP (1984, 1994, 2013, 2017, and 2020).

The genesis potential index is employed to conduct a quantitative diagnostic analysis of the effects of large-scale environmental factors on TC genesis. A modified genesis potential index developed by Murakami and Wang (2010) is applied, which seems to be more capable of representing the variations in TC genesis frequency (Murakami and Wang 2010; Hsu et al. 2014) than the original genesis potential index proposed by Emanuel and Nolan (2004). The modified genesis potential index (GPI) is expressed as

$$\mathrm{GPI} = |10^5\eta|^{3/2}\left(\frac{H}{50}\right)^3\left(\frac{V_p}{70}\right)^3(1 + 0.1\Delta V)^{-2}\left(\frac{-\omega + 0.1}{0.1}\right), \quad (1)$$

where $\eta$ (s$^{-1}$) is the absolute vorticity at 850 hPa, $\Delta V$ (m s$^{-1}$) is the vertical wind shear between the horizontal winds at 200 and 850 hPa, $H$ (%) is the relative humidity at 700 hPa, $V_P$ (m s$^{-1}$) is the potential intensity in terms of maximum wind, and $\omega$ (Pa s$^{-1}$) represents the vertical velocity at 500 hPa. The potential intensity is obtained from sea surface conditions and the vertical profiles of atmospheric variables (Bister and Emanuel 2002; Vecchi and Soden 2007; Bhatia et al. 2022), and its computational details are provided by Bister and Emanuel (2002).

To confirm the impacts of sea surface temperature on the large-scale atmospheric circulation, we conducted the numerical experiments using the Community Earth System Model, version 1.2.1 (CESM1.2.1; Neale et al. 2012; Hurrell et al. 2013). This model is developed by the National Center for Atmospheric Research (NCAR) Atmosphere Model Working Group and is widely used to evaluate global climate changes under different external forcings. Our simulations utilized a finite-volume dynamic core (Neale et al. 2012) with a horizontal resolution of 0.9° × 1.25° and 30 layers in the vertical. The simulations were run with prescribed monthly mean sea surface temperature and sea ice cover.

## 3. Seesaw relationship of TC genesis frequency

Figure 1a presents the time series of TC genesis frequency in the eastern region (0°–20°N, 130°–170°E; blue line) and the western region (0°–25°N, 105°–130°E; green line) of the WNP during July–September from 1970 to 2020. A seesaw relationship of TC genesis frequency between these two regions becomes clearly evident, with a correlation coefficient of −0.52 (significant at the 99% confidence level). When TC genesis frequency in the eastern region of the WNP increases, TC genesis frequency in the western region of the WNP decreases, and vice versa.

It is verified that the result of the correlation analysis is not sensitive to a change in the initial year of the time series. By fixing the end year at 2020 in the analysis, the correlation coefficient between the TC genesis frequency in the eastern and western regions of the WNP is found to be −0.42, −0.48, and −0.52 (significant at the 99% confidence level), corresponding to the initial year being 1960, 1980, and 1990, respectively. It is also shown that the correlation is significant only during the peak TC season (July–September) of the WNP, and it becomes relatively uncertain during the prepeak season (April–June) and postpeak season (October–December). This is primarily due to the smaller sample size of tropical cyclones during these two seasons, with some years even recording no tropical cyclone genesis. Accordingly, our study has focused on the seesaw relationship during the peak season.

To further ensure the robustness of this seesaw relationship, a sensitivity analysis was conducted by varying the eastern boundary of the WNP. Specifically, the time series of TC genesis frequency was compared when the eastern boundary was set at 170°E, 175°E, and 180°. The analysis revealed minimal differences in TC genesis frequency across these boundary definitions. Additionally, the correlation coefficients between the eastern and western regions of the WNP TC genesis frequencies remained significantly negative, with values of −0.49 for 180° and −0.52 for 175°E. These results indicate that the choice of the eastern boundary does not compromise the robustness of the results because of the small sample size of TCs eastward of 170°E in the WNP.

Then, we examine if there is any time lag in this seesaw relationship. As shown in Fig. 1b, the correlation coefficients of the two time series are shown to reach their peaks with a time lag of 0 based on cross-correlation analysis, suggesting an exact out-of-phase relationship of TC genesis frequency between the two regions of the WNP.

## 4. Effects of large-scale environmental factors

To understand the seesaw relationship of TC genesis frequency in the eastern and western regions of the WNP, we perform a composite analysis on the difference in the spatial distribution of TC genesis between the eastern and western active years. An east–west dipole pattern of the TC genesis density over the WNP is then observed, with the pivot located at the longitude of about 130°E (Fig. 2a). Compared with those occurred west of 130°E during the western active years, more TCs tend to occur east of 130°E during the eastern active years. Most of the TCs occurred in the active years are concentrated to the south of 20°N. At the same time, fewer TCs occur near the Philippines and the South China Sea. The dipole pattern is consistent with the fact presented in Fig. 1a.

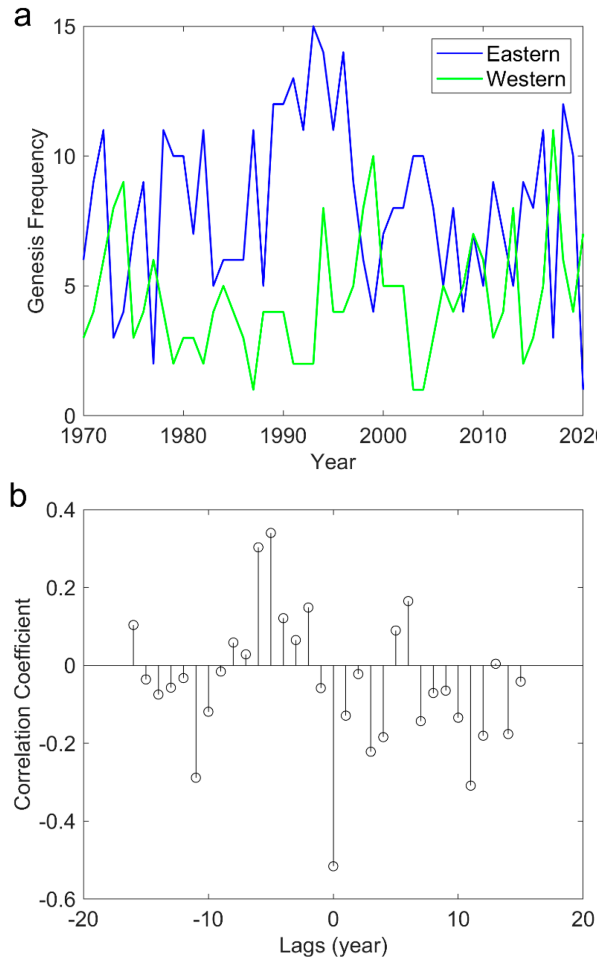


FIG. 1. Out-of-phase relationship of TC genesis frequency between the eastern and western regions of the WNP. (a) Time series of TC genesis frequency in the eastern region (0°–20°N, 130°–170°E; blue line) and the western region (0°–25°N, 105°–130°E; green line) of the WNP in July–September during 1970–2020. (b) The correlation coefficients of the two times series based on cross-correlation analysis.

To understand the mechanism underlying the out-of-phase relationship as shown in Fig. 2a, a composite analysis of the difference in the genesis potential index between the eastern and western active years is also performed, and the result is presented in Fig. 2b. An east–west dipole pattern of the

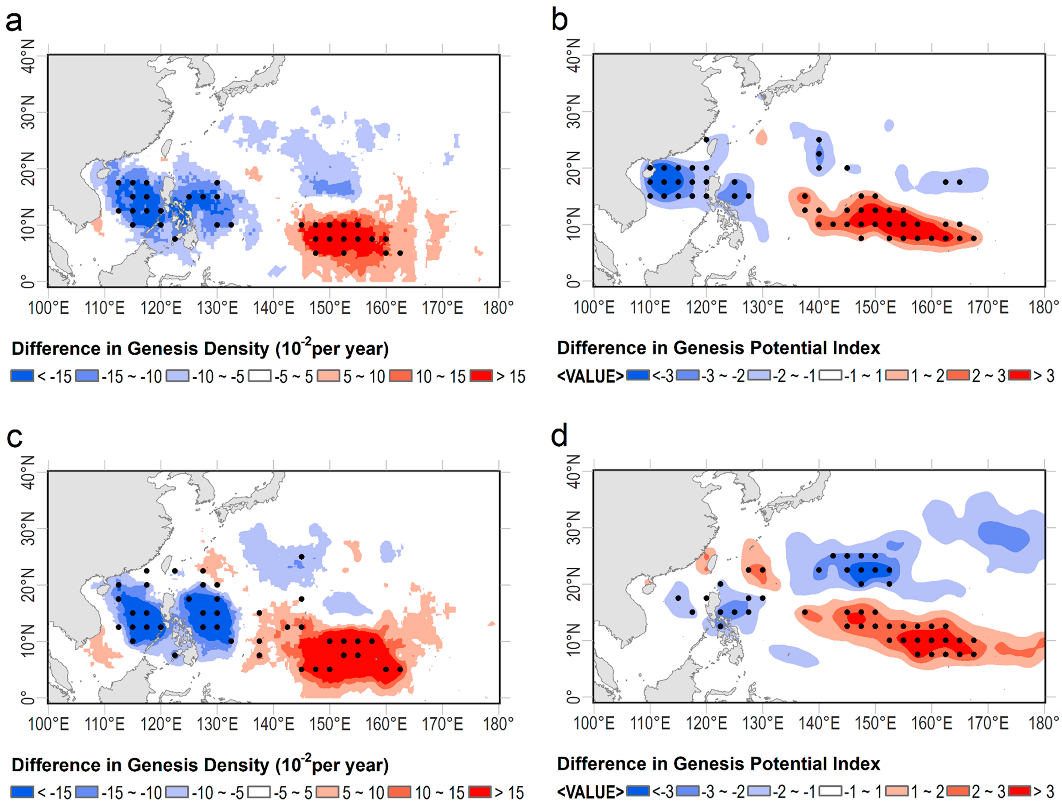


FIG. 2. Changes in the spatial distribution of TC genesis frequency in the WNP and the GPI. Differences in (a) TC genesis density and (b) GPI between the eastern and western active years (eastern active years minus western active years). (c),(d) As in (a) and (b), but with non-ENSO years. Stippling indicates a significant difference at the 95% confidence level.

genesis potential index is obtained, suggesting that the genesis potential index is effective for diagnosing TC genesis.

An additional question arises as to whether this seesaw relationship in TC genesis frequency is influenced by ENSO. To investigate this, we performed a parallel composite analysis, calculating the difference between five non-ENSO active TC years for the eastern region of the WNP and five for the western region of the WNP (see methods). As shown in Figs. 2c and 2d, the out-of-phase relationship in TC genesis between the eastern and western regions of the WNP persists even in the absence of ENSO influence.

The contributions of five factors in the genesis potential index are estimated in the following way. The contribution of factor A is calculated as the fractional change caused by the difference in factor A between the eastern and western active years, i.e., the change in the genesis potential index due to factor A divided by the total change in the genesis potential index. The results obtained indicate that the east–west dipole pattern of the TC genesis is mainly caused by vorticity and relative humidity. The relative contribution of vorticity and relative humidity to the total change in the GPI is approximately 59% and 35%, respectively, in the eastern region of the WNP (jointly 94%) and approximately 35% and 51%, respectively, in the western region of the WNP (jointly 86%). In the eastern region of the WNP, enhanced vorticity in the lower troposphere between 5° and 20°N where most TCs are formed (Fig. 3a) and increased relative humidity in the midtroposphere (Fig. 3b) during the eastern active years provide favorable conditions for TC genesis south of 20°N, while suppressed vorticity and decreased relative humidity in the western region of the WNP are responsible for the reduced TC genesis there. Additionally, the increased atmospheric vorticity and relative humidity south of 20°N in the eastern region of the WNP are consistent with the anomalous ascending motion, while the reduced vorticity and humidity in the western region of the WNP align with the anomalous subsiding motion (Fig. 4). Other factors such as potential intensity and vertical wind shear also affect TC genesis, though their contributions are less important in the present problem.

We have shown that both vorticity and relative humidity contribute to the seesaw relationship of TC genesis frequency between the eastern and western regions of the WNP. It is then of interest to know how atmospheric circulations are related to the particular variations of these factors. For this purpose, we calculate the differences of the horizontal wind between the eastern and western active years. In Fig. 5, an anomalous anticyclone in the WNP is clearly visible at both the 850- and 500-hPa levels, indicating the strengthening of the subtropical high during the eastern active years compared to the western active years. In addition, anticyclonic flows

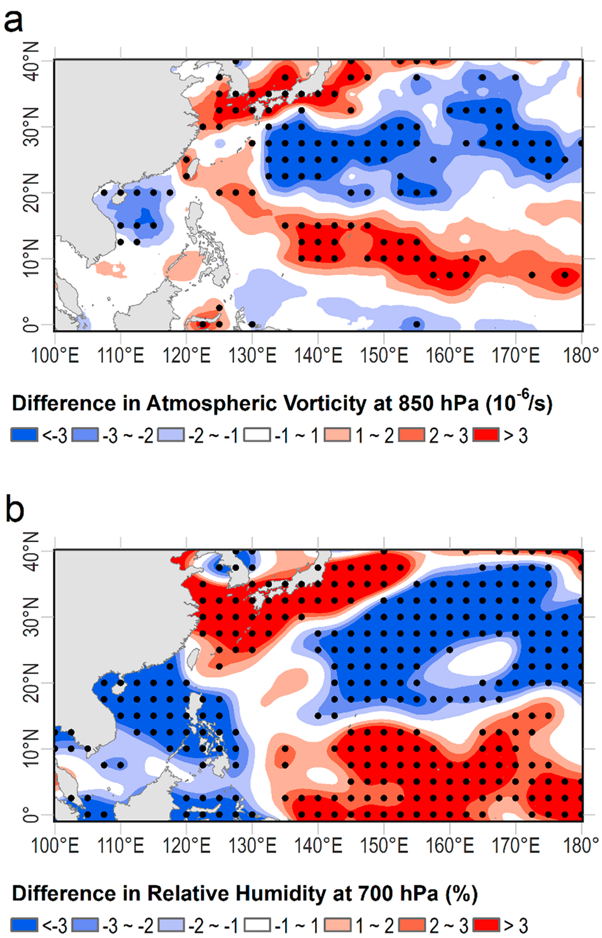


FIG. 3. Changes in the spatial distribution of the large-scale environmental factors. Differences in (a) atmospheric vorticity at 850-hPa level and (b) relative humidity at the 700-hPa level of the troposphere between the eastern and western active years (eastern active years minus western active years). Stippling indicates a significant difference at the 95% confidence level.

prevail at lower to midtroposphere over southeast China, Taiwan, and the South China Sea, leading to suppressed TC genesis frequency over the western portion of the WNP (Fig. 2).

The subtropical high in the WNP is an important atmospheric phenomenon affecting large-scale atmospheric factors related to TC genesis (Ling et al. 2015). Figure 5b shows a strengthened subtropical high in the midtroposphere during the eastern active years, with the positive 500-hPa geopotential height anomalies at approximately 20°N in the eastern region of the WNP. Because the subtropical high is a system with strong anticyclonic vorticity, the anomalous low-latitude easterly winds and anomalous high-latitude westerly winds are generated along the edge of the subtropical high. Similar results could be observed at 850 hPa (Fig. 5a). The strengthened subtropical high associated with the anomalous low-latitude easterly winds strengthens the convergence via wind speed reduction between 130° and 170°E in the lower troposphere and induces an anomalous upward motion in the

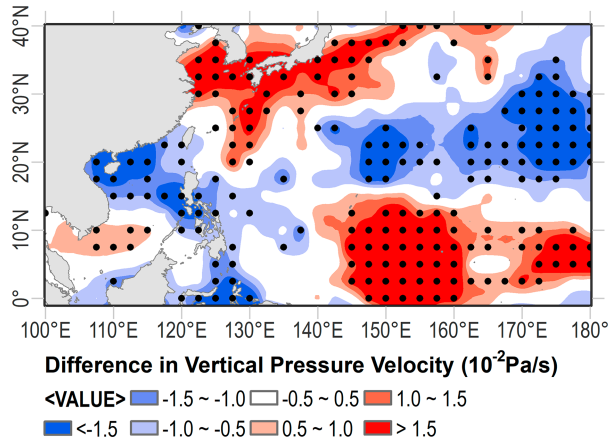


FIG. 4. Changes in the spatial distribution of the vertical velocity (multiplied by −1) at 500 hPa of the troposphere between the eastern and western active years (eastern active years minus western active years).

midtroposphere at the low latitudes (Fig. 4, also see He et al. 2015; Chen et al. 2024). Consistently, the enhanced vorticity and increased humidity are found at approximately 10°N eastward from the Philippine Sea to the date line (Figs. 3a,b), which nearly coincides with the major region of TC genesis in the eastern region of the WNP. The enhanced vorticity and increased humidity provide favorable conditions for TC genesis in the eastern region of the WNP. Furthermore, anticyclonic anomalies prevail in the lower troposphere and reduced water vapor transport in the midtroposphere over the South China Sea and the Philippine Sea is implied, leading to fewer TCs forming in the western region of the WNP.

## 5. Role of sea surface temperature pattern

The formation of the anomalous anticyclone in the western region of the WNP has been considered a result of the SST variations in different ocean basins in previous studies (Wu et al. 2024). The SST warming in the tropical north Indian Ocean (NIO) could trigger an anomalous anticyclone in the WNP in the following boreal summer by inducing a warm tropospheric Kelvin wave (Xie et al. 2009), while the SST cooling in the subtropical WNP could induce an anomalous anticyclone by suppressing local convection (Wang et al. 2003; Fan et al. 2013). Xie et al. (2016) demonstrated that the anomalous anticyclone could arise from interbasin ocean–atmosphere feedback. Furthermore, the strengthened subtropical high in the WNP was demonstrated to be related to the zonal contrast of the NIO warming and WNP cooling in our previous study (Shan et al. 2023).

Figure 6 shows the difference in SST between the eastern and western active years. Compared with the western active years, there is a zonal dipole pattern of the SST over the NIO and WNP during the eastern active years, with a warming of the NIO and a cooling of the WNP. This is consistent with previous studies that showed the significant role of zonal contrast between the NIO warming and WNP cooling in moderating

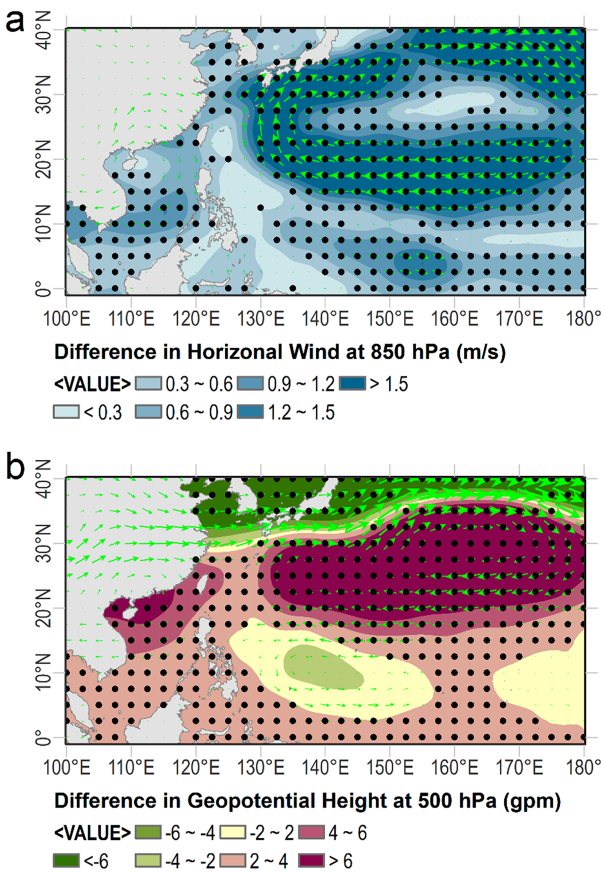


FIG. 5. Changes in atmospheric circulation in the WNP. Differences in (a) horizontal wind at the 850-hPa level and (b) geopotential height at the 500-hPa level of the troposphere between the eastern and western active years (eastern active years minus western active years). Vectors indicate anomalies of the horizontal winds at the corresponding atmospheric levels.

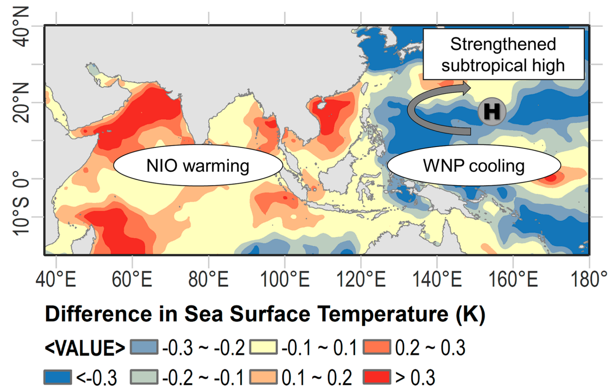


FIG. 6. Schematic diagram explaining the contrasting responses of the eastern and western regions of the WNP TC genesis frequency to the warm NIO and cool WNP. Shadings denote the difference in SST between the eastern and western active years (eastern active years minus western active years).

large-scale atmospheric circulation in the WNP (Xie et al. 2016; Shan et al. 2023).

The composite analysis based on observational data indicates that the seesaw relationship in TC genesis frequency between the eastern and western regions of the WNP is likely to be driven by the warming of the NIO and the cooling of the WNP through moderating the large-scale atmospheric circulation. To test this hypothesis, we conducted numerical simulations using the CESM1.2.1. The control simulation was run for 20 consecutive years, forced by monthly SST climatology from the Hadley Centre (Rayner et al. 2003). The idealized experiment kept the same settings as the control simulation but had a shorter duration (15 yr) and modified SST patterns in specific regions (Fig. 7). We averaged the output over the last 10 years of each simulation to obtain the climatology for a better comparison.

Figure 8 presents the response of observed and simulated horizontal circulation and vertical winds to the anomalous SST pattern. Consistent with observations, the anomalous anticyclone is primarily located north of 20°N in the eastern region of the WNP. This anomalous anticyclone is partly influenced by NIO warming, which triggers a Matsuno–Gill-type response in the troposphere, generating a Kelvin wave wedge that propagates eastward into the WNP. These Kelvin waves could induce the anomalous anticyclonic circulation by causing low-level Ekman divergence (Terao and Kubota 2005; Xie et al. 2009). Additionally, the cooling in the WNP leads to anomalous downward motion and weakened convergence, further supporting the anticyclonic anomalies through an atmospheric Rossby wave response (Li and Zhou 2014; Li et al. 2019; Kim and Kug 2021). The combined effect of NIO warming and WNP cooling leads to the development of the anomalous anticyclone. Additionally, both observational and simulation results indicate anomalous upward flow and enhanced convergence at low latitudes, south of the anticyclonic circulation in the eastern region of the WNP, while anomalous downward motion and reduced convergence are observed in the western region of the WNP, consistent with previous analyses. We also conducted two additional sensitivity experiments, modifying the location and spatial extent of the forcings (Fig. S3). When the position and extent of the idealized forcing were altered, the atmospheric circulation response remained similar (Fig. S4), confirming the robustness of our results. A schematic view of the possible mechanisms related to the contrasting responses of the eastern and western regions of the WNP TC genesis frequency to the warm NIO and cool WNP during the peak season is displayed in Fig. 6.

## 6. Conclusions

We have identified a seesaw relationship of TC genesis frequency between the eastern and western regions of the WNP, with a correlation coefficient of −0.52, which is significant at the 99% confidence level. The result is not sensitive to a change in the initial year of the time series. Based on a composite analysis for the spatial distribution of TC genesis between the eastern and western active years, an east–west

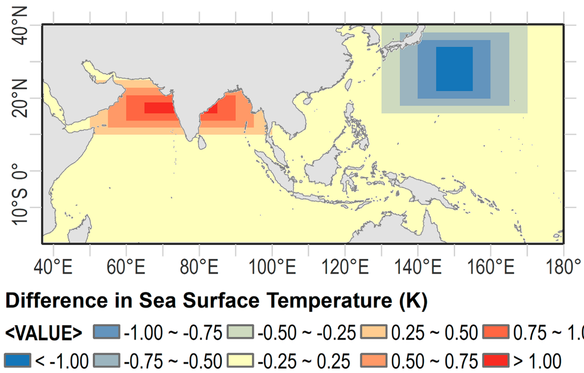


FIG. 7. The distribution of SST forcing in the model over the NIO and WNP.

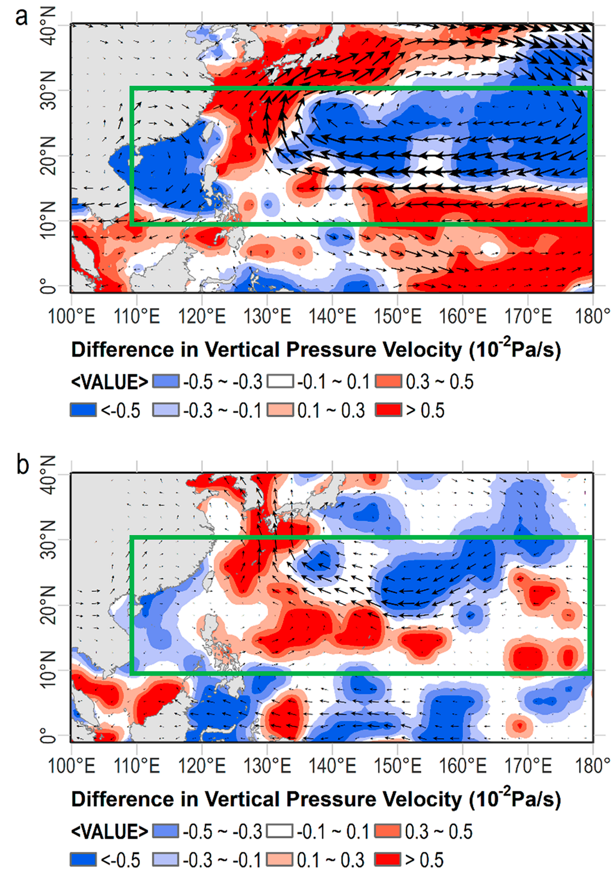


FIG. 8. Comparison of the response of observed and simulated horizontal circulation and vertical winds at 850 hPa to the anomalous SST pattern. (a) The observational result of vertical velocity (multiplied by $-1$) between the eastern and western active years is shown for reference. (b) The numerical result of vertical velocity (multiplied by $-1$) at 850 hPa simulated by the idealized forcing with respect to the control experiment. Red indicates anomalous upward motion, while blue indicates anomalous downward motion. Vectors indicate anomalies of the horizontal winds at the 850-hPa level. The green box indicates the main genesis region of TCs in the WNP.

dipole pattern of TC genesis density over the WNP is found, with the pivot located at the longitude of about 130°E. A similar result is obtained if the composite analysis is performed with respect to the genesis potential index. It is suggested that the seesaw relationship of TC genesis frequency between the eastern and western regions of the WNP is mainly caused by climatological variations in vorticity and relative humidity.

The effect of atmospheric circulations and sea surface temperature patterns are examined. Composite analyses and numerical experiments indicate that a combination of the NIO warming and WNP cooling plays a significant role in driving the seesaw relationship of TC genesis frequency by modulating the subtropical high in the WNP. Compared to the western active years, the subtropical high in the WNP strengthens and extends westward in response to the NIO warming and WNP cooling pattern during the eastern active years. This results in weakened convergence in the lower troposphere and reduced water vapor transport in the midtroposphere over the South China Sea and the Philippine Sea, leading to fewer TCs forming in the western region of the WNP. Conversely, the strengthened subtropical high enhances cyclonic vorticity and relative humidity at the low latitudes eastward from the Philippine Sea to the date line (the primary region for TC genesis in the eastern region of the WNP), thus promoting increased TC genesis.

The current study examines the concurrent effects of a warm Indian Ocean and a cool WNP, which, together, could induce a dipole pattern in TC genesis over the WNP. This contrasts with the previously proposed capacitor effect, which explains the delayed influence of a warm Indian Ocean on suppressed TC activity in the WNP during the summer of the following year, as well as the subsequent development of the subtropical high in the region (Chan 2000; Camargo et al. 2007). To further explore this, we conducted a parallel composite analysis, comparing non-ENSO active TC years from the eastern region of the WNP with non-ENSO active TC years from the western region of the WNP. As shown in Figs. 2c and 2d, the out-of-phase relationship in TC genesis between the eastern and western regions of the WNP persists even in the absence of ENSO influence. In Fig. S5, further analysis of TC genesis density during El Niño and La Niña years reveals a clear east–west dipole pattern, but with a boundary shifted further eastward to approximately 140°E. The east–west dipole pattern of relative humidity during the ENSO composite shows a striking similarity to that in Fig. 3b, which is likely to contribute to the dipole pattern in TC genesis density. Although the sea surface temperature patterns similarly reflect the NIO warming and WNP cooling pattern as in Fig. 6, there is a noticeable warm tongue in the eastern region of the WNP. A notable difference is observed in the 500-hPa geopotential height, where the subtropical high is less pronounced during the ENSO composite. Accordingly, the anomalous vorticity pattern in the ENSO composite provides favorable conditions for TC genesis across the entire WNP, suggesting that it contributes minimally to the dipole pattern of TC genesis. This inconsistency further highlights the contrast between the seesaw pattern observed in our study and the dipole pattern typically associated with ENSO events.

In this study, we also observed potential interdecadal variability in the TC genesis time series (Fig. 1a). To explore this further, we conduct a cross-spectrum analysis to examine the magnitude-squared coherence estimate between the TC genesis time series in the eastern and western regions of the WNP. This coherence estimate, which quantifies the frequency-domain correlation between two signals over specific frequency bands, revealed significant findings. The coherence estimate demonstrates a marked peak at the 6-yr band with a value of 0.75, consistent with the strong correlation on the interannual time scale identified in our study. Additionally, a secondary peak at the 16-yr band with a value of 0.5 suggests a weaker, but still notable, correlation on the interdecadal time scale. To further assess the significance of this correlation on the interdecadal time scale, we apply a 9-yr running mean to the time series, resulting in a correlation coefficient $R = 0.20$, which was not statistically significant ($P > 0.10$). These results imply that the interdecadal variability of the TC genesis time series in the eastern and western regions of the WNP is less pronounced.

*Acknowledgments.* This study is supported by the National Natural Science Foundation of China under Grant 41961144014, the Young Elite Scientists Sponsorship Program by CAST under Grant 2023QNRC001, and the Young Elite Scientists Sponsorship Program by BAST under Grant BYESS2023278.

*Data availability statement.* The International Best Track Archive for Climate Stewardship v04r00 (Knapp et al. 2010) is available at https://www.ncei.noaa.gov/products/international-best-track-archive. The Extended Reconstructed Sea Surface Temperature, version 5, dataset (Huang et al. 2017) is available at https://www.psl.noaa.gov/data/gridded/data.noaa.ersst.v5.html. The fifth major global reanalysis produced by the European Centre for Medium-Range Weather Forecasts (Hersbach et al. 2020) is downloaded from https://cds.climate.copernicus.eu/#!/search?text=ERA5&type=dataset.

## REFERENCES

Bhatia, K., and Coauthors, 2022: A potential explanation for the global increase in tropical cyclone rapid intensification. *Nat. Commun.*, **13**, 6626, https://doi.org/10.1038/s41467-022-34321-6.

Bister, M., and K. A. Emanuel, 2002: Low frequency variability of tropical cyclone potential intensity 1. Interannual to interdecadal variability. *J. Geophys. Res. Atmos.*, **107**, 4801, https://doi.org/10.1029/2001JD000776.

Camargo, S. J., K. A. Emanuel, and A. H. Sobel, 2007: Use of a genesis potential index to diagnose ENSO effects on tropical cyclone genesis. *J. Climate*, **20**, 4819–4834, https://doi.org/10.1175/JCLI4282.1.

Cao, X., R. Wu, J. Xu, Y. Sun, M. Bi, Y. Dai, and X. Lan, 2023a: Coherent variations of tropical cyclogenesis over the North Pacific and North Atlantic. *Climate Dyn.*, **60**, 1385–1396, https://doi.org/10.1007/s00382-022-06381-3.

——, ——, L. Xu, Z. Wang, Y. Sun, Y. Dai, and S. Chen, 2023b: A trans-season out-of-phase relationship of tropical cyclogenesis between the western North Pacific and South China Sea. *J. Climate*, **36**, 3697–3716, https://doi.org/10.1175/JCLI-D-22-0753.1.

——, ——, Z. Wang, X. Lan, Y. Sun, J. Zhao, and Z. Du, 2023c: A zonal see-saw variation of tropical cyclogenesis over the Arabian Sea and Bay of Bengal-South China Sea. *J. Geophys. Res. Atmos.*, **128**, e2023JD038890, https://doi.org/10.1029/2023JD038890.

Chan, J. C. L., 2000: Tropical cyclone activity over the western North Pacific associated with El Niño and La Niña events. *J. Climate*, **13**, 2960–2972, https://doi.org/10.1175/1520-0442(2000)013<2960:TCAOTW>2.0.CO;2.

Chen, K.-C., C.-C. Hong, C.-H. Tsou, and D.-R. Wu, 2024: Present climate and future changes in the annual cycle of TC activity in the WNP investigated by HighResMIP GCMs. *J. Climate*, **37**, 4775–4791, https://doi.org/10.1175/JCLI-D-24-0048.1.

Chen, W., S. Yang, Z. Wu, and F. Cai, 2022: Large-scale atmospheric features favoring the tropical cyclone activity affecting the Guangdong–Hong Kong–Macao Greater Bay area of China. *Environ. Res. Lett.*, **17**, 104057, https://doi.org/10.1088/1748-9326/ac9744.

Chu, P.-S., and H. Murakami, 2022: Climate Variability and Tropical Cyclone Activity. Cambridge University Press, 320 pp.

Emanuel, K. A., and D. S. Nolan, 2004: Tropical cyclone activity and global climate. Preprints, *26th Conf. on Hurricanes and Tropical Meteorology*, Miami, FL, Amer. Meteor. Soc., 10A.2, https://ams.confex.com/ams/26HURR/techprogram/paper_75463.htm.

Fan, L., S.-I. Shin, Q. Liu, and Z. Liu, 2013: Relative importance of tropical SST anomalies in forcing East Asian summer monsoon circulation. *Geophys. Res. Lett.*, **40**, 2471–2477, https://doi.org/10.1002/grl.50494.

He, C., T. Zhou, A. Lin, B. Wu, D. Gu, C. Li, and B. Zheng, 2015: Enhanced or weakened western North Pacific subtropical high under global warming? *Sci. Rep.*, **5**, 16771, https://doi.org/10.1038/srep16771.

Hersbach, H., and Coauthors, 2020: The ERA5 global reanalysis. *Quart. J. Roy. Meteor. Soc.*, **146**, 1999–2049, https://doi.org/10.1002/qj.3803.

Hsu, P.-C., P.-S. Chu, H. Murakami, and X. Zhao, 2014: An abrupt decrease in the late-season typhoon activity over the western North Pacific. *J. Climate*, **27**, 4296–4312, https://doi.org/10.1175/JCLI-D-13-00417.1.

Huang, B., and Coauthors, 2017: Extended Reconstructed Sea Surface Temperature, version 5 (ERSSTv5): Upgrades, validations, and intercomparisons. *J. Climate*, **30**, 8179–8205, https://doi.org/10.1175/JCLI-D-16-0836.1.

Huang, H., W. D. Collins, C. M. Patricola, Y. Ruprich-Robert, P. A. Ullrich, and A. J. Baker, 2023: Contrasting responses of Atlantic and Pacific tropical cyclone activity to Atlantic multidecadal variability. *Geophys. Res. Lett.*, **50**, e2023GL102959, https://doi.org/10.1029/2023GL102959.

Hurrell, J. W., and Coauthors, 2013: The Community Earth System Model: A framework for collaborative research. *Bull. Amer. Meteor. Soc.*, **94**, 1339–1360, https://doi.org/10.1175/BAMS-D-12-00121.1.

Kim, J.-H., C.-H. Ho, and P.-S. Chu, 2010: Dipolar redistribution of summertime tropical cyclone genesis between the Philippine Sea and the northern South China Sea and its possible mechanisms. *J. Geophys. Res.*, **115**, D06104, https://doi.org/10.1029/2009JD012196.

Kim, S., and J.-S. Kug, 2021: Delayed impact of Indian Ocean warming on the East Asian surface temperature variation in boreal summer. *J. Climate*, **34**, 3255–3270, https://doi.org/10.1175/JCLI-D-20-0691.1.

Knapp, K. R., M. C. Kruk, D. H. Levinson, H. J. Diamond, and C. J. Neumann, 2010: The International Best Track Archive for Climate Stewardship (IBTrACS). *Bull. Amer. Meteor. Soc.*, **91**, 363–376, https://doi.org/10.1175/2009BAMS2755.1.

Kossin, J. P., K. R. Knapp, D. J. Vimont, R. J. Murnane, and B. A. Harper, 2007: A globally consistent reanalysis of hurricane variability and trends. *Geophys. Res. Lett.*, **34**, L04815, https://doi.org/10.1029/2006GL028836.

Li, H., F. Xu, J. Sun, Y. Lin, and J. S. Wright, 2019: Subtropical high affects interdecadal variability of tropical cyclone genesis in the South China Sea. *J. Geophys. Res. Atmos.*, **124**, 6379–6392, https://doi.org/10.1029/2018JD029874.

Li, R. C. Y., and W. Zhou, 2014: Interdecadal change in South China Sea tropical cyclone frequency in association with zonal sea surface temperature gradient. *J. Climate*, **27**, 5468–5480, https://doi.org/10.1175/JCLI-D-13-00744.1.

Li, S., and W. Mei, 2024: Spatiotemporal variability of tropical cyclone genesis density in the northwest Pacific. *J. Climate*, **37**, 1111–1129, https://doi.org/10.1175/JCLI-D-22-0868.1.

Ling, Z., G. Wang, and C. Wang, 2015: Out-of-phase relationship between tropical cyclones generated locally in the South China Sea and non-locally from the Northwest Pacific Ocean. *Climate Dyn.*, **45**, 1129–1136, https://doi.org/10.1007/s00382-014-2362-7.

Maue, R. N., 2009: Northern Hemisphere tropical cyclone activity. *Geophys. Res. Lett.*, **36**, L05805, https://doi.org/10.1029/2008GL035946.

Murakami, H., and B. Wang, 2010: Future change of North Atlantic tropical cyclone tracks: Projection by a 20-km-mesh global atmospheric model. *J. Climate*, **23**, 2699–2721, https://doi.org/10.1175/2010JCLI3338.1.

——, T. L. Delworth, W. F. Cooke, M. Zhao, B. Xiang, and P.-C. Hsu, 2020: Detected climatic change in global distribution of tropical cyclones. *Proc. Natl. Acad. Sci. USA*, **117**, 10 706–10 714, https://doi.org/10.1073/pnas.1922500117.

Neale, R. B., and Coauthors, 2012: Description of the NCAR community atmosphere model (CAM 5.0). NCAR Tech. Note NCAR/TN-486+STR, 268 pp., https://www2.cesm.ucar.edu/models/cesm1.1/cam/docs/description/cam5_desc.pdf.

Rayner, N. A., D. E. Parker, E. B. Horton, C. K. Folland, L. V. Alexander, D. P. Rowell, E. C. Kent, and A. Kaplan, 2003: Global analyses of sea surface temperature, sea ice, and night marine air temperature since the late nineteenth century. *J. Geophys. Res.*, **108**, 4407, https://doi.org/10.1029/2002JD002670.

Schreck, C. J., III, K. R. Knapp, and J. P. Kossin, 2014: The impact of best track discrepancies on global tropical cyclone climatologies using IBTrACS. *Mon. Wea. Rev.*, **142**, 3881–3899, https://doi.org/10.1175/MWR-D-14-00021.1.

Shan, K., and X. Yu, 2020a: Interdecadal variability of tropical cyclone genesis frequency in western North Pacific and South Pacific Ocean basins. *Environ. Res. Lett.*, **15**, 064030, https://doi.org/10.1088/1748-9326/ab8093.

——, and ——, 2020b: Enhanced understanding of poleward migration of tropical cyclone genesis. *Environ. Res. Lett.*, **15**, 104062, https://doi.org/10.1088/1748-9326/abaf85.

——, and ——, 2021: Variability of tropical cyclone landfalls in China. *J. Climate*, **34**, 9235–9247, https://doi.org/10.1175/JCLI-D-21-0031.1.

——, P.-S. Chu, and X. Yu, 2023: Interdecadal change of tropical cyclone translation speed during peak season in South China Sea: Observed evidence, model results, and possible mechanism. *J. Climate*, **36**, 4531–4541, https://doi.org/10.1175/JCLI-D-22-0704.1.

Sobel, A. H., A. A. Wing, S. J. Camargo, C. M. Patricola, G. A. Vecchi, C.-Y. Lee, and M. K. Tippett, 2021: Tropical cyclone frequency. *Earth's Future*, **9**, e2021EF002275, https://doi.org/10.1029/2021EF002275.

Terao, T., and T. Kubota, 2005: East-west SST contrast over the tropical oceans and the post El Niño western North Pacific summer monsoon. *Geophys. Res. Lett.*, **32**, L15706, https://doi.org/10.1029/2005GL023010.

Tu, J.-Y., J.-M. Chen, P.-H. Tan, and T.-L. Lai, 2022: Seasonal contrasts between tropical cyclone genesis in the South China Sea and westernmost North Pacific. *Int. J. Climatol.*, **42**, 3743–3756, https://doi.org/10.1002/joc.7442.

Vecchi, G. A., and B. J. Soden, 2007: Effect of remote sea surface temperature change on tropical cyclone potential intensity. *Nature*, **450**, 1066–1070, https://doi.org/10.1038/nature06423.

Walsh, K. J. E., and Coauthors, 2015: Hurricanes and climate: The U.S. CLIVAR Working Group on hurricanes. *Bull. Amer. Meteor. Soc.*, **96**, 997–1017, https://doi.org/10.1175/BAMS-D-13-00242.1.

Wang, B., R. Wu, and T. Li, 2003: Atmosphere–warm ocean interaction and its impacts on Asian–Australian monsoon variation. *J. Climate*, **16**, 1195–1211, https://doi.org/10.1175/1520-0442(2003)16<1195:AOIAII>2.0.CO;2.

Wang, C., and S.-K. Lee, 2009: Co-variability of tropical cyclones in the North Atlantic and the eastern North Pacific. *Geophys. Res. Lett.*, **36**, L24702, https://doi.org/10.1029/2009GL041469.

——, L. Wang, X. Wang, D. Wang, and L. Wu, 2016: North-south variations of tropical storm genesis locations in the Western Hemisphere. *Geophys. Res. Lett.*, **43**, 11 367–11 374, https://doi.org/10.1002/2016GL071440.

——, B. Wang, L. Wu, and J.-J. Luo, 2022: A seesaw variability in tropical cyclone genesis between the western North Pacific and the North Atlantic shaped by Atlantic multidecadal variability. *J. Climate*, **35**, 2479–2489, https://doi.org/10.1175/JCLI-D-21-0529.1.

Wu, R., Y. Yang, and X. Cao, 2019: Respective and combined impacts of regional SST anomalies on tropical cyclogenesis in different sectors of the western North Pacific. *J. Geophys. Res. Atmos.*, **124**, 8917–8934, https://doi.org/10.1029/2019JD030736.

Wu, S., W. Lin, L. Dong, F. Song, S. Yang, Z. Lu, and X. Hu, 2024: Role of SST in seasonal western North Pacific anomalous anticyclone: Insights from AMIP simulations in CMIP6. *Geophys. Res. Lett.*, **51**, e2023GL107080, https://doi.org/10.1029/2023GL107080.

Wu, Z., C. Hu, L. Lin, W. Chen, L. Huang, Z. Lin, and S. Yang, 2023: Unraveling the strong covariability of tropical cyclone activity between the Bay of Bengal and the South China Sea. *npj Climate Atmos. Sci.*, **6**, 180, https://doi.org/10.1038/s41612-023-00506-z.

Xie, S.-P., K. Hu, J. Hafner, H. Tokinaga, Y. Du, G. Huang, and T. Sampe, 2009: Indian Ocean capacitor effect on Indo–western Pacific climate during the summer following El Niño. *J. Climate*, **22**, 730–747, https://doi.org/10.1175/2008JCLI2544.1.

——, Y. Kosaka, Y. Du, K. Hu, J. Chowdary, and G. Huang, 2016: Indo-western Pacific Ocean capacitor and coherent climate anomalies in post-ENSO summer: A review. *Adv. Atmos. Sci.*, **33**, 411–432, https://doi.org/10.1007/s00376-015-5192-6.

Yuan, J., Y. Gao, D. Feng, and Y. Yang, 2019: The zonal dipole pattern of tropical cyclone genesis in the Indian Ocean influenced by the tropical Indo-Pacific Ocean Sea surface temperature anomalies. *J. Climate*, **32**, 6533–6549, https://doi.org/10.1175/JCLI-D-19-0042.1.